An increase of the spall strength in aluminum, copper, and Metglas at strain rates larger than 10^7 s^{-1}

E. Moshe, S. Eliezer, E. Dekel, A. Ludmirsky, Z. Henis,[a] M. Werdiger, and I. B. Goldberg
Department of Plasma Physics, Soreq NRC, Yavne 81800, Israel

N. Eliaz and D. Eliezer
Department of Materials Engineering, Ben–Gurion University, Beer-Sheva, Israel

(Received 23 July 1997; accepted for publication 19 January 1998)

Measurements of the dynamic spall strength in aluminum, copper, and Metglas shocked by a high-power laser to hundreds of kilobars pressure are reported. The strain rates in these experiments are of the order of 10^7 s^{-1}, which cannot be reached in impact experiments. The free-surface velocity behavior associated with spallation is characterized by oscillations caused by the reverberations of the spall layer. An optically recording velocity interferometer system was developed to measure the free-surface velocity time history. This diagnostic method has the advantages of being a noninterfering system and produces a highly accurate continuous measurement in time. The spall strength was calculated from the free-surface velocity as a function of the strain rate. The results show a rapid increase in the spall strength, suggesting that a critical phenomenon occurs at strain rates $\sim 10^7$ s^{-1}, expressed by the sudden approach to the theoretical value of the spall strength. © *1998 American Institute of Physics.* [S0021-8979(98)08308-X]

I. INTRODUCTION

This paper presents an experimental study of the dynamic behavior of materials shocked to hundreds of kilobars pressure. In the experiments reported here, the measurement of the resistance of solids to dynamic fracture relies on the detection of the spall phenomenon.

A high-power laser pulse induces a pressure wave in a solid target. The peak of the pressure wave results in a shock front, while its rear decreasing slope induces a rarefaction wave into the shocked material. The failure mode occurs upon the reflection of the shock wave from the free surface. When the shock wave reaches the free surface, the compressed material expands freely and accelerates the surface to the velocity $u_{fs}=2\cdot u_p$, where u_p is the particle velocity (the mass velocity in the shocked material). The expansion leads to material straining, and therefore, to a deceleration of the surface. The superposition of the two rarefaction waves, the tail of the initial pressure wave and tensile stress wave, running in opposite directions, yields a residual stress whose amplitude increases with the distance to the free surface. When this stress exceeds the material strength, spalling occurs in a plane parallel to the free surface. The expanded material of the spall region bounces back from the spall surface, generating another pressure wave moving in the direction of the original shock wave and accelerates the free surface. This second pressure reaches the free surface and is reflected as a stress wave. The wave reverberations in the spall region are superposed to the surface velocity at the moment of the rupture and are then damped down due to dissipative losses. The spall pressure or the material strength is determined from the measurement of the free-surface velocity time history.

An optically recording velocity interferometer system (ORVIS) was developed to measure the time evolution of the free surface.[1,2] This diagnostic method provides an accurate continuous measurement of the surface velocity, having also the advantage of being noninterfering with the motion of the shocked target.

We used aluminum, copper, and Metglas 2605TCA ($Fe_{78}B_{13}Si_9$), an amorphous alloy, as targets. The spall strengths were measured as a function of the strain rate. For the laser-induced shock waves reported here, strain rates of 10^7 s^{-1} are realized, higher than the strain rates reached in experiments using impact of a projectile on a target, explosive generator, or powder gun. The experiments are described in Sec. II. The spall pressure is calculated in Sec. III from the measured time dependence of the free-surface velocity, using the acoustic approximation. In addition, the time dependence of the pressure inside the target was calculated by integrating the equations of motion describing the interaction between the two rarefaction waves.

The fracture morphology was studied by means of scanning electron microscopy. The mechanism of fracture in aluminum and copper is dimple rupture (microvoid coalescence), typical to ductile materials. The spall in Metglas is characterized by a vain pattern and a cellular pattern, indicating the brittleness of the material.

The results of the experiments reported here show a rapid increase of the dynamic spall strength with the strain rate, at strain rates of the order of 10^7 s^{-1}. This behavior is different compared to the much smaller spall strength–strain rate dependence[3] up to strain rates of 10^7 s^{-1}.

[a]Electronic mail: henis@ndc.soreq.gov.il

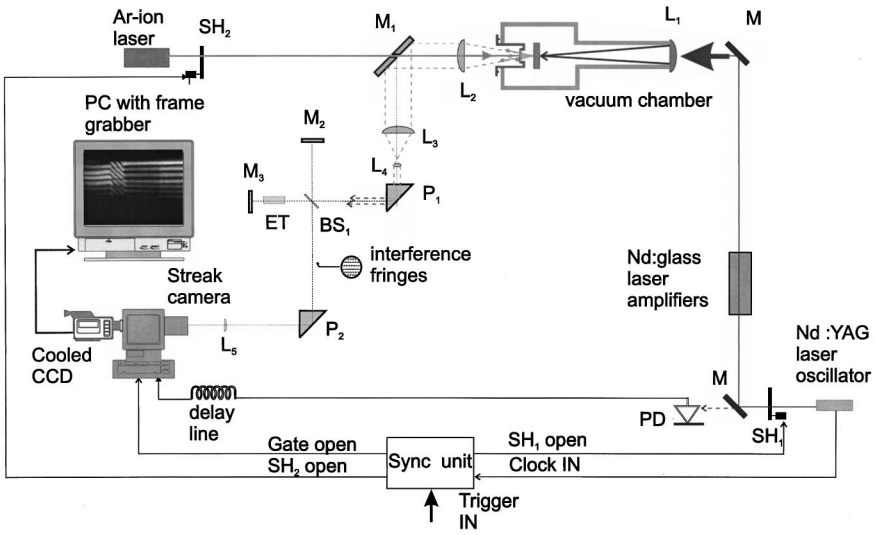

FIG. 1. Schematic description of the ORVIS and the laser-induced shock waves experiment; M_1, M_2, and M_3: mirrors; L_1, L_2, L_3, L_4, and L_5: lenses; BS_1 and BS_2: beam splitters; ET: étalon; P_1 and P_2: prisms; SH_1 and SH_2: shutters; and PD: photodiodes.

II. EXPERIMENTS

The experimental setup for the free-surface velocity measurements was described in Ref. 2 and is shown in Fig. 1. The main laser system that generates the shock waves is based on a Continuum NY-60 Nd:YAG oscillator followed by one triple-passed and one double-passed glass amplifier. The laser operates at a wavelength of 1.06 μm, pulse width (full width at half maximum) of 2 and 5 ns and energy in the range (10–80) J and is focused to a spot diameter in the range (200–1000) μm. The laser irradiance in the experiments reported here was of the order of 10^{13} W/cm^2. The diagnostic interferometric system consists of an argon–ion laser focused to 50 μm on the rear surface, aligned accurately with the spot of the main laser beam. The light reflected from the moving free surface undergoes a Doppler shift proportional to the velocity of the free surface. The light is collected, collimated, and reflected into a Michelson interferometer. The beam splitter divides the beam into two nonequal legs. An étalon is placed in the route of one of the legs. The two beams are back reflected and then recombine. The recombination of the two beams produces an interference pattern of parallel fringes. These fringes are generated from light, which was reflected from the target at two different times. Therefore, when the target is moving the fringes are shifted. The interference pattern is imaged by a cylindrical lens to a set of bright spots on the entrance slit of a streak camera. The time resolution of most of the experiments reported here was 70 ps. The interference pattern is analyzed with an image processing system, including a cool charge-coupled device camera, a frame grabber, and a PC.

The velocity history of the moving free surface is determined from the change in the interference pattern. The fringes move in a direction perpendicular to their orientation when the velocity changes with the direction depending on the sign of the velocity change. The velocity of the moving surface is related to the vertical position $y(t)$ of the interference pattern as a function of time:[1,4,5]

$$u_{\mathrm{fs}}(t)=\frac{\lambda\cdot c}{4\cdot L_e\cdot\left(n-\frac{1}{n}\right)}\cdot\frac{y(t)}{(1+\delta)\cdot d}. \tag{1}$$

λ is the laser wavelength, d is the fringe spacing, L_e is the length of the étalon, n its index of refraction, and c is the speed of light in vacuum. $(1+\delta)$ is a correction term due to the wavelength dependence of the refractive index of the étalon material. In the experiments here, $\delta=0.034$ at the argon laser wavelength 514.5 nm.

The fringe pattern representing the free-surface velocity, in an experiment with a 5 ns, 68 J laser pulse focused to a 500 μm diam spot and a 50 μm thick aluminum target is shown in Fig. 2. Time is increasing from left to right. The full time scale of Fig. 2 is 5.6 ns and the distance between two fringes (the fringe constant) is 0.301 km/s. The fringes are parallel to the time axis before the free surface undergoes acceleration, then the fringe pattern starts shifting, indicating the acceleration of the free surface. Figure 3 shows the fringe pattern of an aluminum target, measured in an experiment with a 7 ns, 60 J laser pulse focused to a 500 μm diam spot, when the free-surface velocity is monitored during 30 ns. The fringe constant is 0.435 km/s. The time resolution in this experiment was of the order of 0.5 ns. The signature of the wave reverberations in the spall region are seen in the oscillations of the fringe pattern in Fig. 3. The fringe pattern representing the free-surface velocity, in an experiment with a 2.2 ns, 34 J laser pulse focused to a 250 μm diam spot and a 38 μm thick copper target is shown in Fig. 4. In addition to metallic materials, we studied the spall phenomenon in amorphous alloys. The fringe pattern of a 25 μm thick Metglas target irradiated with a 2.2 ns, 26 J laser pulse focused to a 500 μm diam spot is shown in Fig. 5. The fringe constant corresponding to the fringe pattern shown in Figs. 4 and 5 is 0.301 km/s. One can see that the amplitude of the oscillations in the fringe pattern is higher in Metglas than for the two metallic materials studied here.

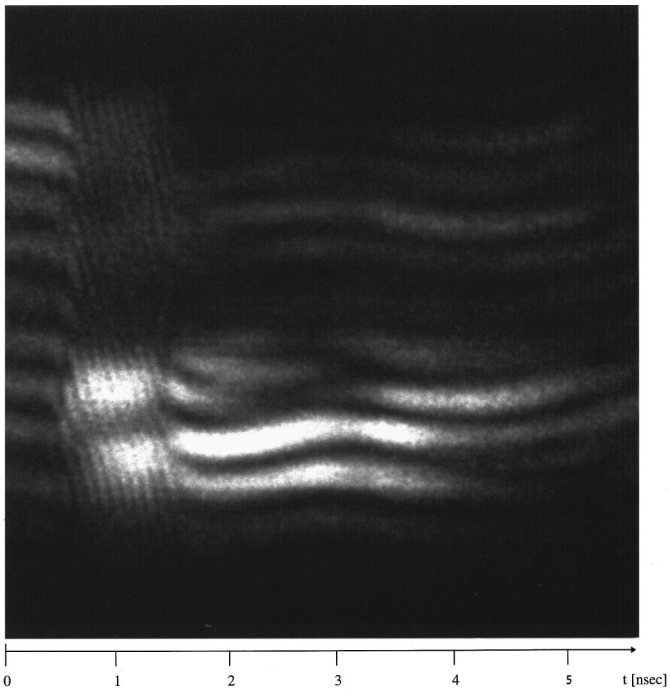

FIG. 2. The interference pattern obtained with the ORVIS in an experiment with a 50 μm thick aluminum foil irradiated by a 68 J, 5 ns laser pulse. The full time scale is 5.6 ns and the fringe constant (the distance between two fringes) 0.301 km/s.

In all the experiments reported here the spot size was by almost an order of magnitude larger than the foil thickness, resulting in the one-dimensional geometry of the shock waves propagating through the target.

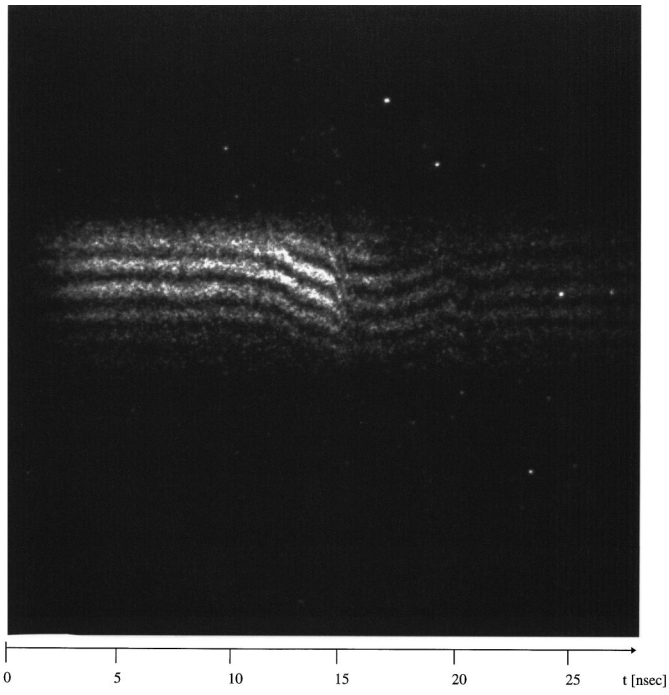

FIG. 3. The interference pattern obtained with the ORVIS in an experiment with a 50 μm thick aluminum foil irradiated by a 60 J, 7 ns laser pulse. The full time scale is 30 ns and the fringe constant 0.435 km/s.

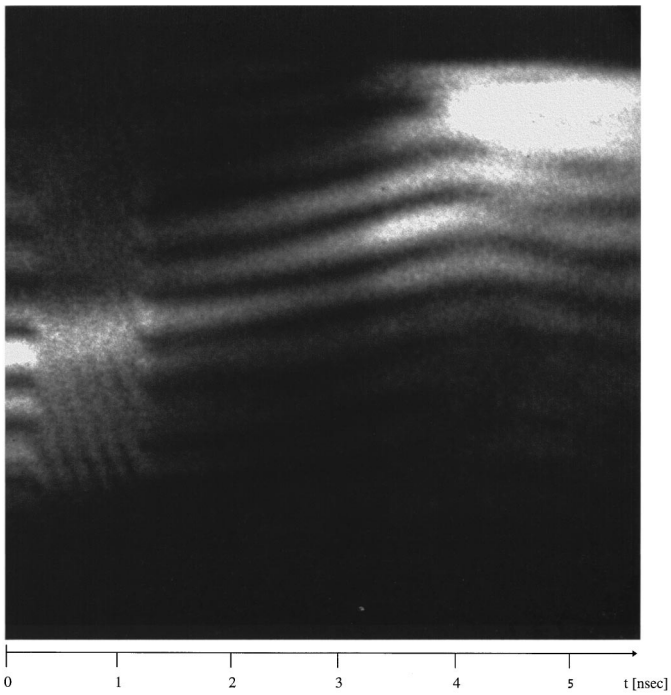

FIG. 4. The interference pattern obtained with the ORVIS in an experiment with a 38 μm thick copper foil irradiated by a 34 J, 2.2 ns laser pulse. The full time scale is 5.6 ns and the fringe constant 0.301 km/s.

III. THE SPALL PRESSURE CALCULATION

The spall strength was determined from the measured time dependence of the free surface by two methods: First, in the acoustic approximation[6] the spall strength is

$$P_{\text{spall}} = \tfrac{1}{2}\rho_0 c(u_{\max} - u_{\min}). \tag{2}$$

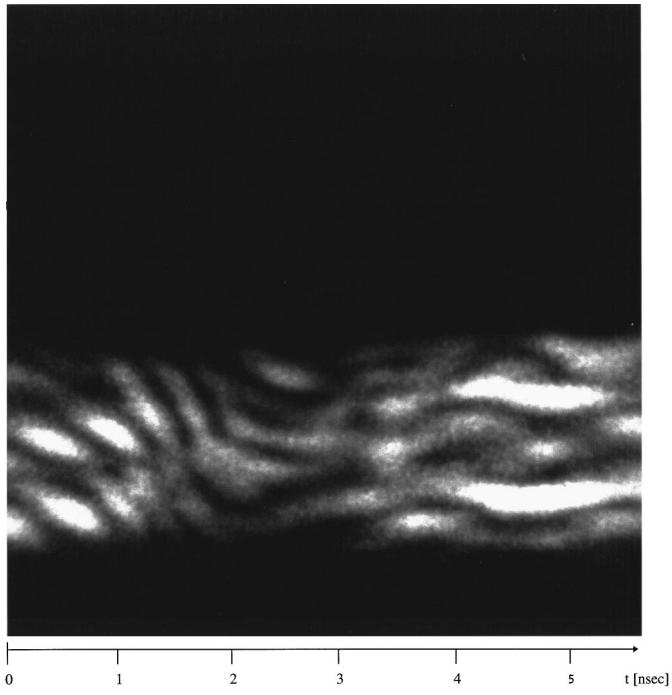

FIG. 5. The interference pattern obtained with the ORVIS in an experiment with a 25 μm thick Metglas foil irradiated by a 26 J, 2.2 ns laser pulse. The full time scale is 5.6 ns and the fringe constant 0.301 km/s.

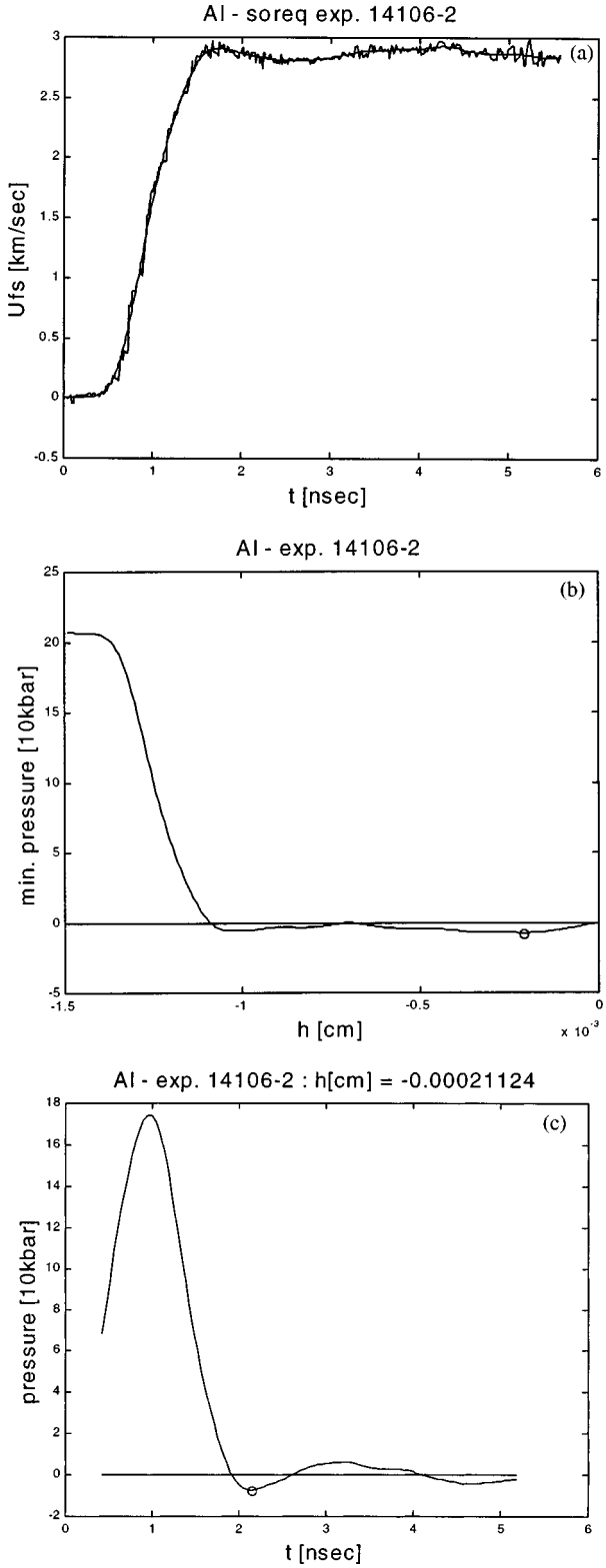

FIG. 6. (a) The free-surface velocity as function of time corresponding to the fringe pattern displayed in Fig. 2. (b) The minimum pressure as a function of time vs the Lagrangian coordinate for the experiment shown in Fig. 2. (c) The pressure at the spall position as a function of time for the experiment shown in Fig. 2.

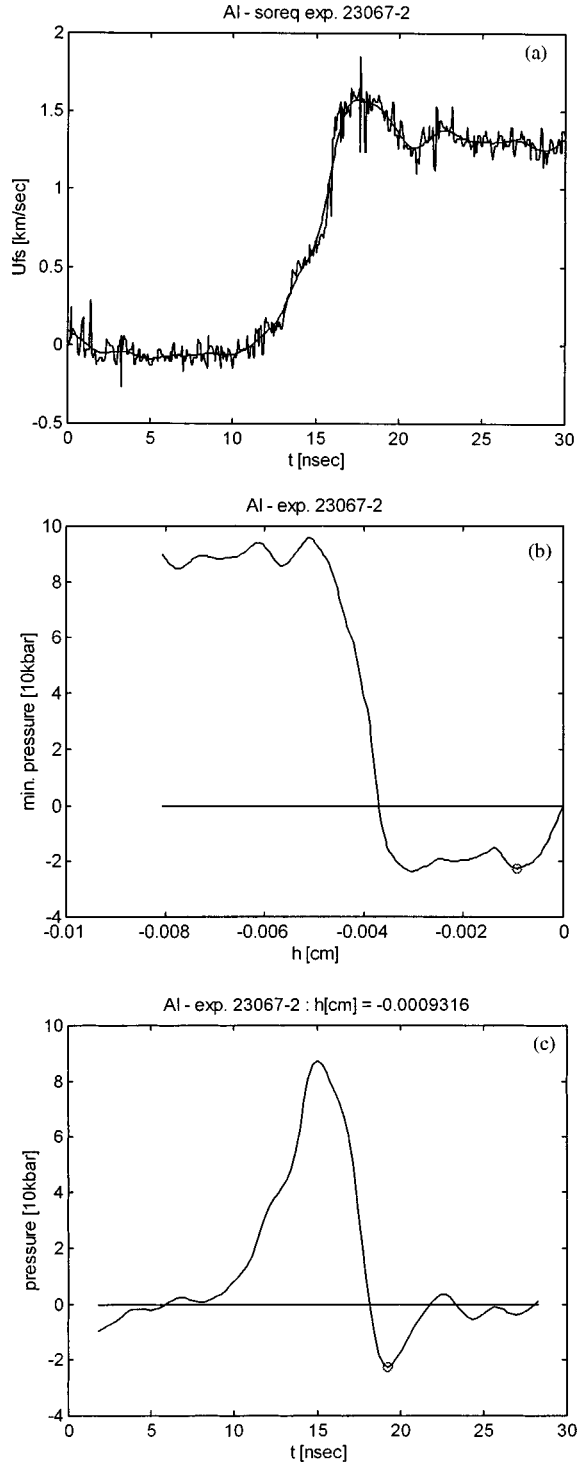

FIG. 7. (a) The free-surface velocity as function of time corresponding to the fringe pattern displayed in Fig. 3. (b) The minimum pressure as a function of time vs the Lagrangian coordinate for the experiment shown in Fig. 3. (c) The pressure at the spall position as a function of time for the experiment shown in Fig. 3.

ρ_0 is the initial density of the target, c is the sound velocity, $u_{\max}$ is the peak velocity of the free surface, and $u_{\min}$ is the first minimum in the free-surface profile.

The time dependence of the pressure inside the target was calculated by integrating the equations of motion describing the interaction between the two rarefaction waves. The momentum conservation is given by

$$\frac{\partial u}{\partial t}+\frac{1}{\rho_0}\frac{\partial P}{\partial h}=0. \tag{3}$$

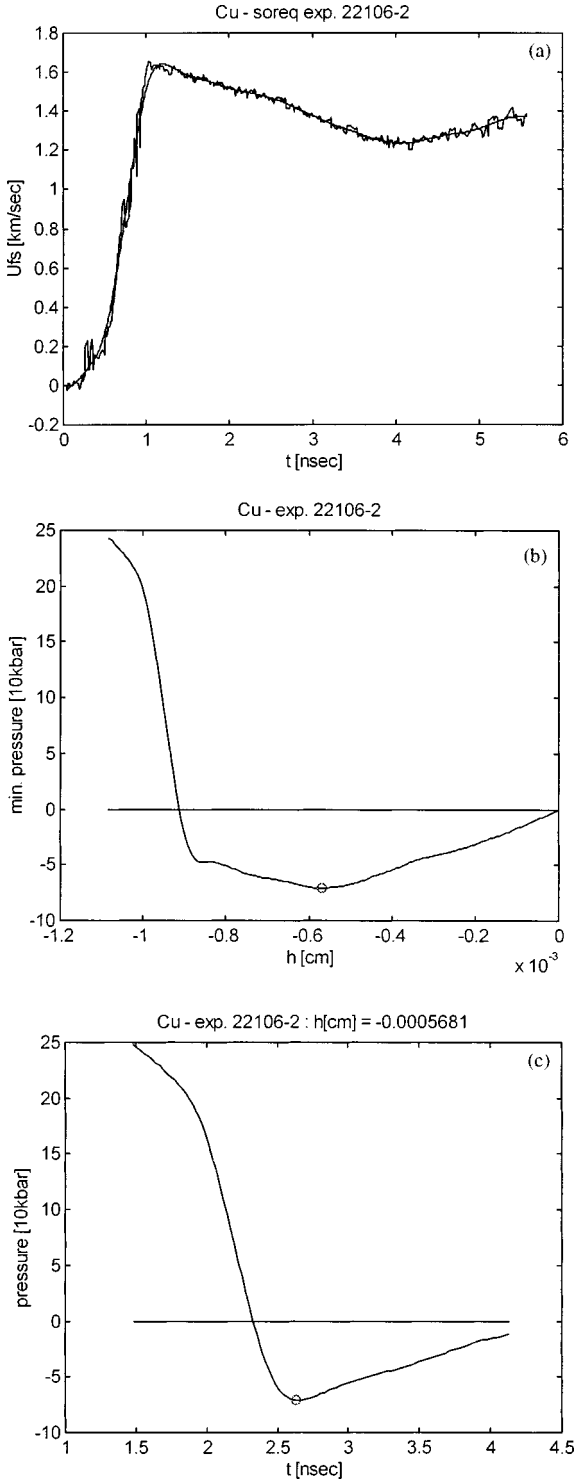

FIG. 8. (a) The free-surface velocity as function of time corresponding to the fringe pattern displayed in Fig. 4. (b) The minimum pressure as a function of time vs the Lagrangian coordinate for the experiment shown in Fig. 4. (c) The pressure at the spall position as a function of time for the experiment shown in Fig. 4.

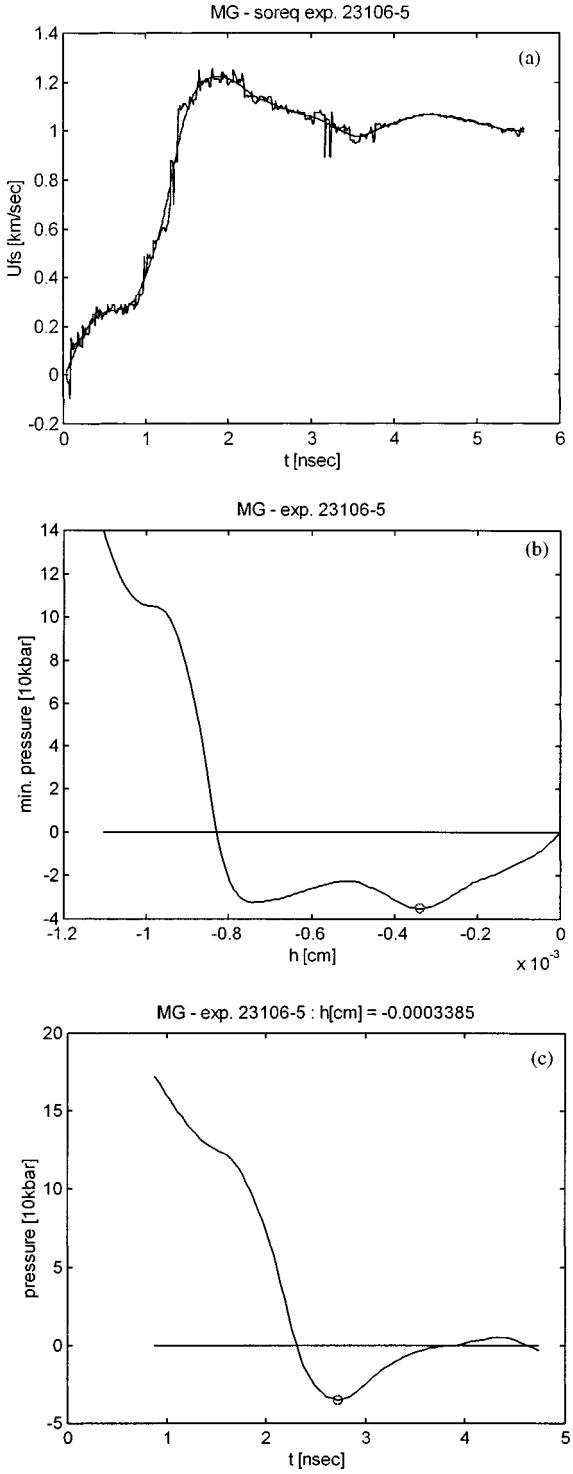

FIG. 9. (a) The free-surface velocity as function of time corresponding to the fringe pattern displayed in Fig. 5. (b) The minimum pressure as a function of time vs the Lagrangian coordinate for the experiment shown in Fig. 5. (c) The pressure at the spall position as a function of time for the experiment shown in Fig. 5.

h is the Lagrangian coordinate, $h=\int_0^x(\rho/\rho_0)dx$, u is the particle velocity, P is the pressure, ρ_0 is the initial density, and ρ is the density.

A general solution of the wave equation describing the two waves running in opposite directions is

$$P(h,t)=f_1\left(\frac{h}{c}+t\right)+f_2\left(\frac{h}{c}-t\right). \tag{4}$$

Using the boundary condition $P=0$ at the free surface, $h=0$, we obtain:

TABLE I. Summary of the shots displayed in Figs. 2–9.

Target material	Target thickness (μm)	Laser energy (J)	Laser pulse duration (ns)	Streak camera full time scale (ns)	Fringe constant (km/s)	Shot displayed in Figs.
Al	50	68	5	5.6	0.301	2,6
Al	50	60	7	30	0.435	3,7
Cu	38	34	2.2	5.6	0.301	4,8
Metglas	25	26	2.2	5.6	0.301	5,9

$$P(h,t)=f_1\left(\frac{h}{c}+t\right)-f_1\left(\frac{h}{c}-t\right). \tag{5}$$

The pressure in the target as a function of the free-surface velocity measured in the experiment is obtained by using Eqs. (3) and (5):

$$P(h,t)=-\frac{\rho_0 c}{2}\left[u_{\mathrm{fs}}\left(\frac{h}{c}+t\right)-u_{\mathrm{fs}}\left(-\frac{h}{c}+t\right)\right]. \tag{6}$$

The spall strength expression given by Eq. (2) results from Eq. (6) if

$$\frac{h_{\mathrm{spall}}}{c}+t_{\mathrm{spall}}=t(u_{\max}),\quad -\frac{h_{\mathrm{spall}}}{c}+t_{\mathrm{spall}}=t(u_{\min}). \tag{7}$$

A time and length scale for the spall result

$$\begin{aligned} t_{\mathrm{spall}}&=\tfrac{1}{2}\cdot[t(u_{\max})+t(u_{\min})],\\ h_{\mathrm{spall}}&=\tfrac{1}{2}\cdot c\cdot[t(u_{\max})-t(u_{\min})]. \end{aligned} \tag{8}$$

The strain rate was calculated by

$$\dot{\epsilon}=\left.\frac{du_{\mathrm{fs}}}{dt}\right|_{t=t_{\mathrm{spall}}}\cdot\frac{1}{2c}. \tag{9}$$

The sound velocity c for aluminum and copper was taken from the SESAME equation of state.[7] The sound velocity for Metglas was taken from Ref. 8.

The data analysis for the experiments displayed in Figs. 2–5 is shown in Figs. 6–9. Figure 6(a) shows the experimental data, i.e., the free-surface velocity of the aluminum foil as a function of time. The minimum pressure (for all times), calculated using Eq. (6), at every Lagrangian coordinate h, is plotted in Fig. 6(b). The coordinate corresponding to the first minimum in Fig. 6(b) is identified with the spall position. The minimum pressure as the function of time at the spall position is plotted in Fig. 6(c). The data analysis obtained from the fringe pattern of aluminum shown in Fig. 3, is plotted in Fig. 7. In this experiment, the free-surface velocity is measured during 30 ns (while in the other experiments only about 6 ns).

Figure 8 displays the measured free-surface velocity, the minimum pressure versus the Lagrangian coordinate, and the minimum pressure as a function of time corresponding to the copper fringe pattern shown in Fig. 4. The results for the Metglas target are plotted in Fig. 9. It is seen that for this amorphous alloy the pullback velocity ($u_{\max}-u_{\min}$) is a larger fraction of the peak free-surface velocity than for the metallic targets. Table I summarizes the shots displayed in Figs. 2–9.

IV. RESULTS AND DISCUSSION

The spall pressure was calculated by the method described above. The spall pressures for aluminum and copper are plotted as a function of the strain rate, in Figs. 10 and 11. These figures display also other experimental results[9,10] performed at lower strain rates than the range studied here and the theoretical[11] spall strength of solids. The data shown in Figs. 10 and 11 can be fitted to

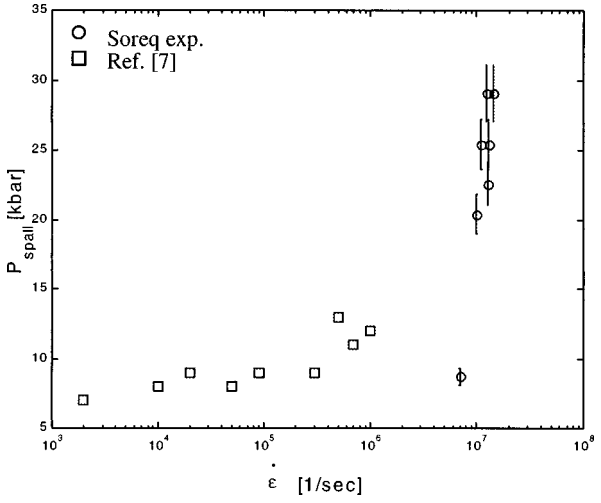

FIG. 10. The spall strength as a function of the strain rate in aluminum.

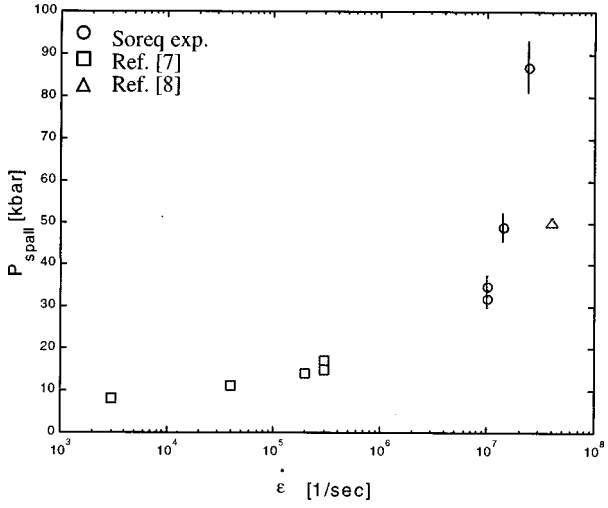

FIG. 11. The spall strength as a function of the strain rate in copper.

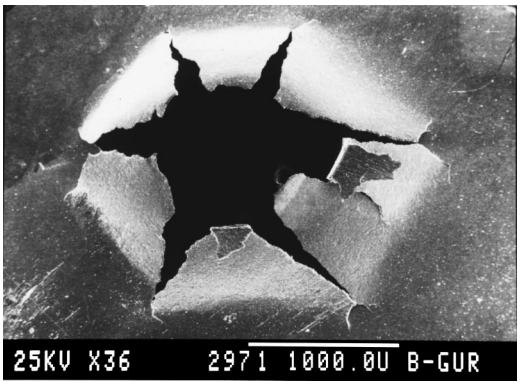

FIG. 12. The rear surface in Metglas at a magnification of 36, showing the spall morphology.

$$P_{\text{spall}} = P_0 \cdot \arctan(\dot{\epsilon}\tau_0 + \epsilon_0) + P_1 . \tag{10}$$

For example, the fit parameters for aluminum are

$$P_0 = 99 \text{ kbar}, \quad P_1 = 14 \text{ kbar},$$

$$\epsilon_0 = 0.04, \quad \tau_0 = 4.7 \times 10^{-9} \text{ s}.$$

The spall strength in Metglas $P_{\text{spall}} = (58.5 \pm 4.1)$ kbar was calculated using the sound velocity $c = 4$ km/s, estimated from the experiments.

P_{th}, the theoretical spall strength of solids considers interatomic interactions forces only and can be estimated[11] from U_{coh}, the cohesive energy per gram, the normal density ρ_0, and the bulk modulus B_0:

$$P_{\text{th}} = \sqrt{\frac{U_{\text{coh}} B_0 \rho_0}{8}}. \tag{11}$$

For Al and Cu Eq. (11) yields 171 and 285 kbar accordingly, about one order of magnitude more than the spall strength measured at strain rates in the range $(10^3 - 10^6)\text{s}^{-1}$. This occurs due to the fact that the mechanical properties of solids are controlled by lattice imperfections and dislocations, which weaken the materials.

It is seen in Fig. 10 that the spall strength varies slowly with the strain rate in the range $(10^3 - 10^6)\text{s}^{-1}$. For example, in aluminum the spall pressure changes from 7 to 15 kbar in the strain rate range $(10^3 - 10^6)\text{s}^{-1}$.

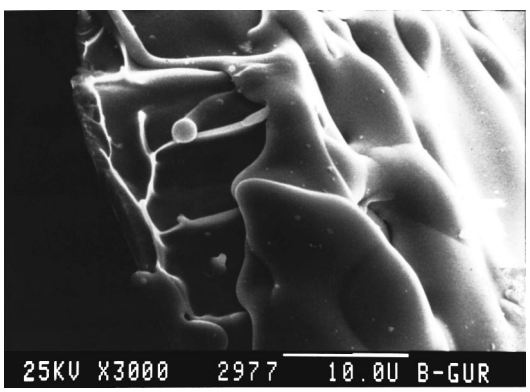

FIG. 13. Vein pattern in the fracture surface in Metglas at a magnification of 3000.

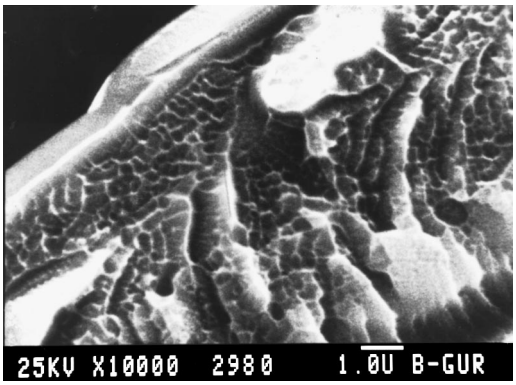

FIG. 14. Cellular pattern in the fracture surface in Metglas at a magnification of 10 000.

In contrast to this behavior, in the experiments reported here, a rapid increase in the spall strength of Al from 7 to 43 kbar is observed in the strain rate range $(9 \times 10^6 - 4 \times 10^7)\text{s}^{-1}$. The measured spall strength in copper increased from 30 to 90 kbar in the strain rate range $(10^7 - 2.5 \times 10^7)\text{s}^{-1}$.

The results of the experiments reported here suggest that a critical phenomenon occurs at strain rates of about 10^7 s^{-1}, expressed by a sudden approach to the theoretical value of the spall strength.

The fracture morphology of the spall was studied by means of scanning electron microscopy. Figure 12 shows a picture of the Metglas rear surface with a magnification of 36. Cracks and secondary cracks are seen in the fracture surface, indicating the brittleness of the material. Parts of the fracture surface in Metglas are seen in Figs. 13 and 14 at magnification of 3000 and 10 000. The absence of dislocations in the amorphous alloy prevents significant plastic deformation before fracture. The deformation in amorphous metals is classified into homogeneous flow and nonhomogeneous flow. The nonhomogeneous flow is characterized by the veins pattern seen in Fig. 13. Figure 14 shows that some of the fracture displays a cellular pattern. This kind of pattern was reported after hydrogenation of amorphous $Fe_{40}Ni_{38}Mo_4B_{18}$ and was related to an embrittlement as a result of heterogeneous nucleation of local plastic

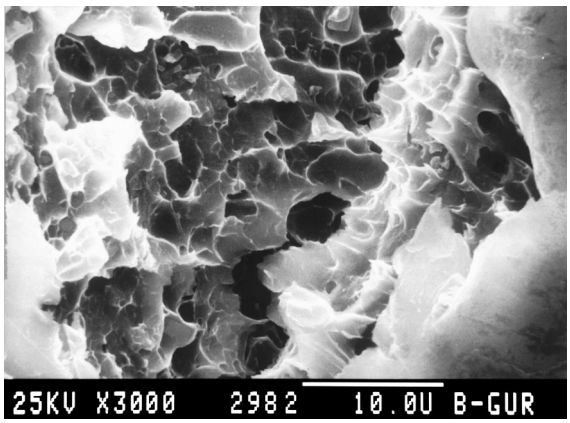

FIG. 15. Microvoid pattern in the fracture surface in aluminum at a magnification of 3000.

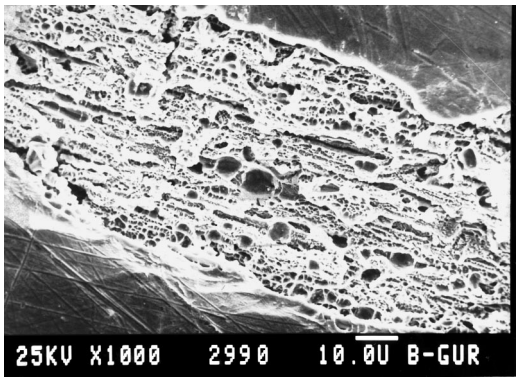

FIG. 16. Microvoid pattern in the fracture surface in copper at a magnification of 1000.

deformation.[12] The fracture surface in aluminum and copper, which are fcc metals, are seen in Figs. 15 and 16 at magnifications 3000 and 1000. These figures show that the mechanism of fracture seems to be dimple rupture (microvoid coalescence), typical to ductile materials. The microvoids nucleate in the material at areas of localized high plastic deformation, such as that associated with inclusions and grain boundaries. As the load on the material increases, the microvoids grow, coalesce, and eventually form a continuous fracture surface. The microvoids in copper are smaller than in aluminum, suggesting a larger value of the spall strength in copper than in aluminum.

ACKNOWLEDGMENTS

The authors thank Dr. B. Arad and Dr. Y. Paiss for very helpful and stimulating discussions. The authors thank S. Maman for his skillful technical assistance.

[1] D. D. Bloomquist and A. A. Sheffield, J. Appl. Phys. **54**, 1717 (1983).
[2] E. Moshe, E. Dekel, Z. Henis, and S. Eliezer, Appl. Phys. Lett. **69**, 1379 (1996).
[3] V. E. Fortov, V. V. Kostin, and S. Eliezer, J. Appl. Phys. **70**, 4524 (1991).
[4] K. Baumung and J. Singer, in *Physics of Intense Light Ion Beams and Production of High Energy Density in Matter*, Annual Report 1994 (Forschungzentrum Karlsruhe GmBH, Karlsruhe, 1995), p. 88.
[5] L. M. Barker and K. W. Schuler, J. Appl. Phys. **45**, 3692 (1974).
[6] G. I. Kanel and V. E. Fortov, Adv. Mech. **10**, 3 (1987).
[7] T-4 Handbook of Material Properties Data Bases, edited by K. S. Holian, LA-10160-MS, Los Alamos, UC-34 (1984).
[8] Z. Kaczkowski and H. S. Nam, in *Magnetic Properties of Amorphous Metals*, edited by A. Hernando, V. Madurga, M. C. Sanchez-Trulillo, and M. Vazquez (Elsevier Science, Amsterdam, 1987), p. 139.
[9] A. V. Bushman, G. I. Kanel', A. L. Ni, and V. E. Fortov, *Intense Dynamic Loading of Condensed Matter* (Taylor & Francis, Washington D.C., 1993).
[10] D. L. Paisley, R. H. Warnes, and R. A. Kopp, in *Shock Waves in Condensed Matter*, edited by S. C. Schmidt, R. D. Dick, J. W. Forbes, and D. G. Tasker (Elsevier Science, New York, 1991).
[11] D. E. Grady, J. Mech. Phys. Solids **3**, 353 (1988).
[12] J. J. Lin and T. P. Perng, Metall. Mater. Trans. A **26**, 197 (1995).